Scripta Materialia 164 (2019) 62–65

Contents lists available at ScienceDirect

Scripta Materialia

journal homepage: www.elsevier.com/locate/scriptamat

High electrostrain with high Curie temperature in $BiFeO_3$-$BaTiO_3$-based ceramics

Lei Wang [a,b], Ruihong Liang [a,*], Zhiyong Zhou [a], Xianlin Dong [a,c,**]

[a] Key Laboratory of Inorganic Functional Materials and Devices, Shanghai Institute of Ceramics, Chinese Academy of Sciences, 1295 Dingxi Road, Shanghai 200050, People's Republic of China
[b] University of Chinese Academy of Sciences, Beijing 100049, People's Republic of China
[c] State Key Laboratory of High Performance Ceramics and Superfine Microstructure, Shanghai Institute of Ceramics, Chinese Academy of Sciences, Shanghai 200050, People's Republic of China

ARTICLE INFO

Article history:
Received 27 November 2018
Accepted 21 January 2019
Available online xxxx

Keywords:
$BiFeO_3$-based ceramics
Electrostrain
High T_C
Vancancy

ABSTRACT

Here, we report a high unipolar electrostrain (0.45%) with a high Curie temperature (T_C = 410 °C) in lead-free (1-*x*)(0.67$BiFeO_3$–0.33$BaTiO_3$)-*x*$Sr_{0.8}La_{0.1}\square_{0.1}TiO_{2.95}$ (□ represents the A-site vacancy) piezoceramics with x = 0.02. $Sr_{0.8}La_{0.1}\square_{0.1}TiO_{2.95}$ was introduced to construct a relaxor ferroelectric state. The obtained unipolar strain was thermally stable, and the variation from room temperature to 100 °C was only 10%. Systematic electromechanical and Raman spectra measurements revealed a composition driven phase transition from classical ferroelectric to relaxor ferroelectric phases and distorted internal stress field. This work provides a novel strategy to obtain high electrostrain in high temperature piezoceramics.

Piezoelectric ceramics are the core components in smart piezoelectric actuator systems, which have been widely used in precision positioners, ultrasonic motors, and adaptive mechanical dampers, etc. [1–4] For these actuator applications, the most important parameter is the strain induced by electric field, namely electrostrain. Generally, there are four different kinds of mechanisms of electrostrain that exist in piezoelectric ceramics. The intrinsic two mechanisms include converse piezoelectric effect and electrostriction, originating from field-induced lattice distortion and displacement of ions, respectively. However, their strain values are commonly small. For conventional piezoelectric (e.g., Pb(Zr,Ti)O_3, (PZT)) and some relaxor ferroelectric ceramics with large electrostrictive coefficients (e.g., $Pb(Mg_{1/3}Nb_{1/3})O_3$), the induced strain is of the order of 0.1% [4,5]. Two extrinsic mechanisms, including non-180° domain switching and phase transition, can be used to realize high electrostrain, since large crystal distortion occurs during both cases [2]. Recently, a high electrostrain value of 1.3% has been observed in $BiFeO_3$-$PbTiO_3$-$LaFeO_3$ ceramics based on the combined phase transition and non-180° domain switching mechanisms [6]. This may also provide a practical strategy for the design of high performance lead-free piezoelectric ceramics.

A large lattice strain is the basis to realize large electrostrain. $BiFeO_3$-$PbTiO_3$ exhibits a giant spontaneous lattice strain (c/a-1) of 0.18, one order higher than $BaTiO_3$ (~0.01), making it a good candidate as a host material [6,7]. It should be noted that large lattice distortion exists in itself of bismuth ferrite ($BiFeO_3$). First principle calculation on $BiFeO_3$ in the tetragonal phase shows a lattice strain (~0.22) even higher than $BiFeO_3$-$PbTiO_3$ [8,9]. Unfortunately, the largest electrostrain obtained in $BiFeO_3$ ceramics was only 0.35%, indicating a large energy barrier during domain switching [10]. Therefore, a low free energy is needed to switch the ferroelectric domain to utilize the spontaneous lattice strain. It is accepted that the composition driven morphotropic phase boundary (MPB) can help to reduce the internal energy barrier during domain switching [4,11,12]. Moreover, the formation of relaxor ferroelectrics can flatten the free energy profile, and facilitate domain switching [13,14]. Large electrostrain has been reported in lead-free $Bi_{0.5}Na_{0.5}TiO_3$-$Bi_{0.5}K_{0.5}TiO_3$-based ceramics with above features [15,16]. However, the $Bi_{0.5}Na_{0.5}TiO_3$-based materials show low depolarization temperature (~150 °C) and large hysteresis [17–19]. It is thus urgent to develop lead-free piezoelectric ceramics that have both high electrostrain and high Curie temperatures.

In this study, we chose high Curie temperature 0.67$BiFeO_3$–0.33$BaTiO_3$ ceramics at the morphotropic phase boundary as the base composition. Previous works showed that the 0.67$BiFeO_3$–0.33$BaTiO_3$ ceramic have a high T_C around 450 °C [11]. A-site deficient $Sr_{0.8}La_{0.1}\square_{0.1}TiO_{2.95}$ (□ represents the A-site vacancy) was added as the modifier to form relaxor ferroelectric states. La-doped $SrTiO_3$ was generally accepted a relaxor ferroelectric with typical dielectric relaxation behavior [20]. A-site vacancy (V_A) was introduced to create a randomly distributed local polarization field. Systematic electrical characterizations showed a composition driven phase transition from classical ferroelectric to relaxor ferroelectric phases. More importantly,

* Corresponding author.
** Correspondence to: X. Dong, State Key Laboratory of High Performance Ceramics and Superfine Microstructure, Shanghai Institute of Ceramics, Chinese Academy of Sciences, Shanghai 200050, People's Republic of China.
E-mail addresses: liangruihong@mail.sic.ac.cn (R. Liang), xldong@mail.sic.ac.cn (X. Dong).

https://doi.org/10.1016/j.scriptamat.2019.01.028
1359-6462/

a high unipolar strain of 0.45% with a high Curie temperature of 410 °C was obtained in samples with 0.02 mol% $Sr_{0.8}La_{0.1}\square_{0.1}TiO_{2.95}$.

$(1\text{-}x)(0.67BiFeO_3\text{–}0.33BaTiO_3)\text{-}xSr_{0.8}La_{0.1}\square_{0.1}TiO_{2.95}$ ($x = 0.00, 0.01, 0.02, 0.03\ 0.04$; abbreviated as BFBT-100*x*SLT) ceramics were prepared by conventional solid state method. The starting materials, including Bi_2O_3 (99.99%), Fe_2O_3 (99%), $BaCO_3$ (99%), $SrCO_3$ (99%), La_2O_3 (99.95%) and TiO_2 (99.8%), were weighted and ball milled for 24 h. After drying, the slurries were calcined at 800 °C for 5 h at a rate of 5 °C/min and then remilled for another 24 h to obtain a fine powder size. The dried powders were pressed into pellets with a 13 mm diameter and a 1 mm thickness at a pressure of 200 MPa with PVA (polyvinyl alcohol) as the binder. The pellets were heated to 600 °C for 2 h to burn off the binder. After cooling, they were sintered at 1010–1040 °C for 5 h.

Structural quantification was performed by powder X-ray diffraction measurements (XRD, Rigaku D/max 2550, Japan) using Cu Kα radiation. Surface morphologies were observed using a SEM (Hitachi TM3000, Japan). Raman spectroscopy was measured by Renishaw InVia Raman system, UK. The dielectric properties were measured using an E4980A impedance analyzer (Agilent, USA). For electrical measurements, the samples were thinned to 0.3 mm. Silver paste was coated on both surfaces of samples and fired at 650 °C for 30 min. Ferroelectric properties and electrostrain were measured by a ferroelectric analyzer connected with a laser interferometer (TF2000, aix-ACCT, Germany).

Fig. 1a and b shows the room temperature XRD patterns of unpoled BFBT-100*x*SLT ceramics. All the patterns indexed belong to perovskite phases, revealing no any secondary phases in the composition range. As the SLT contents increasing, nearly no shift of the peak position occurs, indicating small variation of their lattice parameters (Fig. 1a). The similar ionic radii of the La^{3+} ($R_{La^{3+}} = 1.36$, CN = 12) and Sr^{2+} ($R_{Sr^{2+}} = 1.44$, CN = 12) compared to Bi^{3+} ($R_{Bi^{3+}} = 1.39$, CN = 12) at the A site [21], may contribute to the high structural stability during the SLT addition. The detailed lattice symmetry is commonly determined by the (110) peak splitting of pseudocubic phase. The enlarged patterns of 2θ ~ 31.5° are shown in Fig. 1b. As *x* increased from 0.00 to 0.04, the broad single (110) peak continuously split into two peaks. Pure $0.67BiFeO_3\text{–}0.33BaTiO_3$ ceramics are widely accepted to be located on the phase boundary between pseudocubic (*Pm-3m*) and rhombohedral (*R3c*) phases [11]. The splitting XRD peaks clearly indicate the coexistence of pseudocubic and rhombohedral symmetries, and systematic improved rhombohedral phases with SLT addition.

The dielectric constants (ε_r) and loss (tanδ) as a function of temperature for BFBT-100*x*SLT ceramics are shown in Fig. 1c and d. The maximum dielectric constants (ε_m) progressively decreased and the temperatures at which (T_m) shifted toward lower temperatures as SLT contents increasing. The dielectric loss tanδ declined with SLT addition, indicating the enhanced electrical insulation. For $x \le 0.02$, the samples exhibited high T_C of over 400 °C, which is desired for high temperature piezoelectric applications. For $x = 0.03$ and 0.04, significant diffuse dielectric behavior can be observed, demonstrating that the ceramics are typical relaxor ferroelectrics. The diffuseness of dielectric constants can be described by a modified Curie-Weiss relationship $1/\varepsilon\text{-}1/\varepsilon_m = (T - T_m)^\gamma/C$ at $T > T_m$, where C is the Curie constant and γ is the diffuseness degree (1 for normal ferroelectric, and 2 for complete diffuse phase transition) [22]. The fitted dielectric behaviors are shown in Fig. 1d. The diffuseness degree improved from 1.73 to 1.94 for *x* increased from 0.00 to 0.04. The diffuse phase transition is associated with many factors, such as structural disorder, microscopic heterogeneities and stoichiometric fluctuations. Here the A-site multivalences of $Sr_{0.8}La_{0.1}\square_{0.1}TiO_{2.95}$ can disrupt the long-range polar order at the microscopic area, and the introduced A-site vacancies further brought the stoichiometric fluctuations, which may explain the promoted diffuseness degree.

Noted that the amount of polar rhombohedral phases increased with SLT addition, which was in contradiction with the promoted diffuseness degree. One possible explanation is that the polar rhombohedral phases are exist on nanoscale of the matrix. Previous transmission electron microscopy studies have confirmed such nanoscale coexistence in $BiFeO_3\text{-}BaTiO_3$ ceramics [23]. Thus random electric field rises as the nanoscale polar phase contents increasing. Similar effects have been observed in $(Sr_{0.8}Bi_{0.1}\square_{0.1})TiO_{2.95}$ modified BNT-based ceramics [16]. The relaxor-like behavior can provide a low energy barrier for domain switching, and is benefit for obtaining high electrostrain.

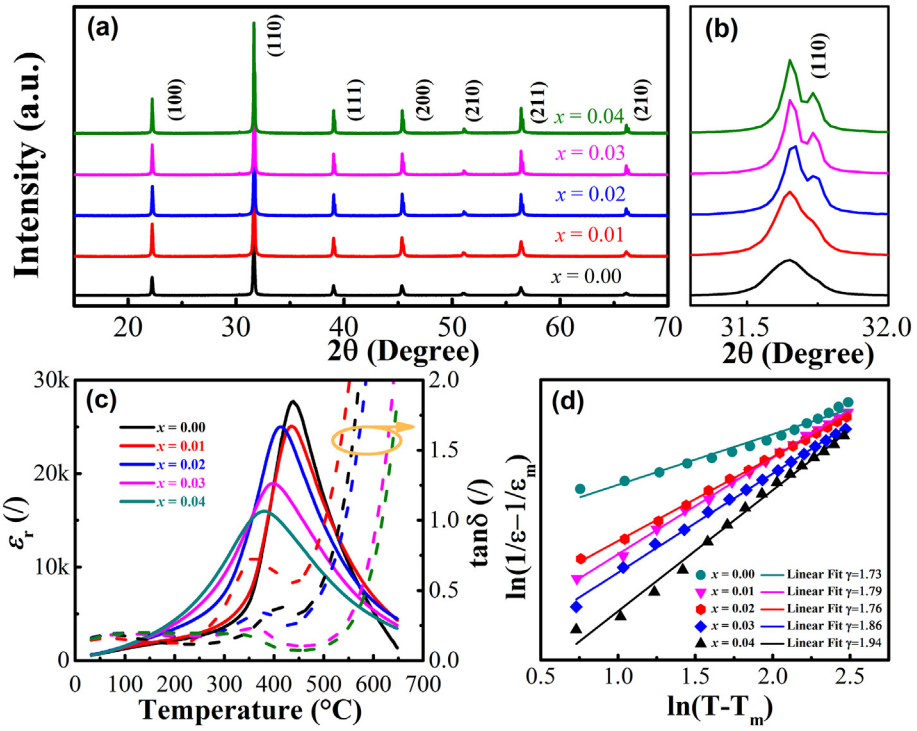

Fig. 1. X-ray diffraction patterns of BFBT-100*x*SLT ceramics with (a) 2θ = 15–70° (b) 2θ = 31.25–32.00°. (c) Temperature dependent dielectric constant and loss and (d) $\ln(1/\varepsilon\text{-}1/\varepsilon_m)$ versus $\ln(T\text{-}T_m)$ plots for BFBT-100*x*SLT.

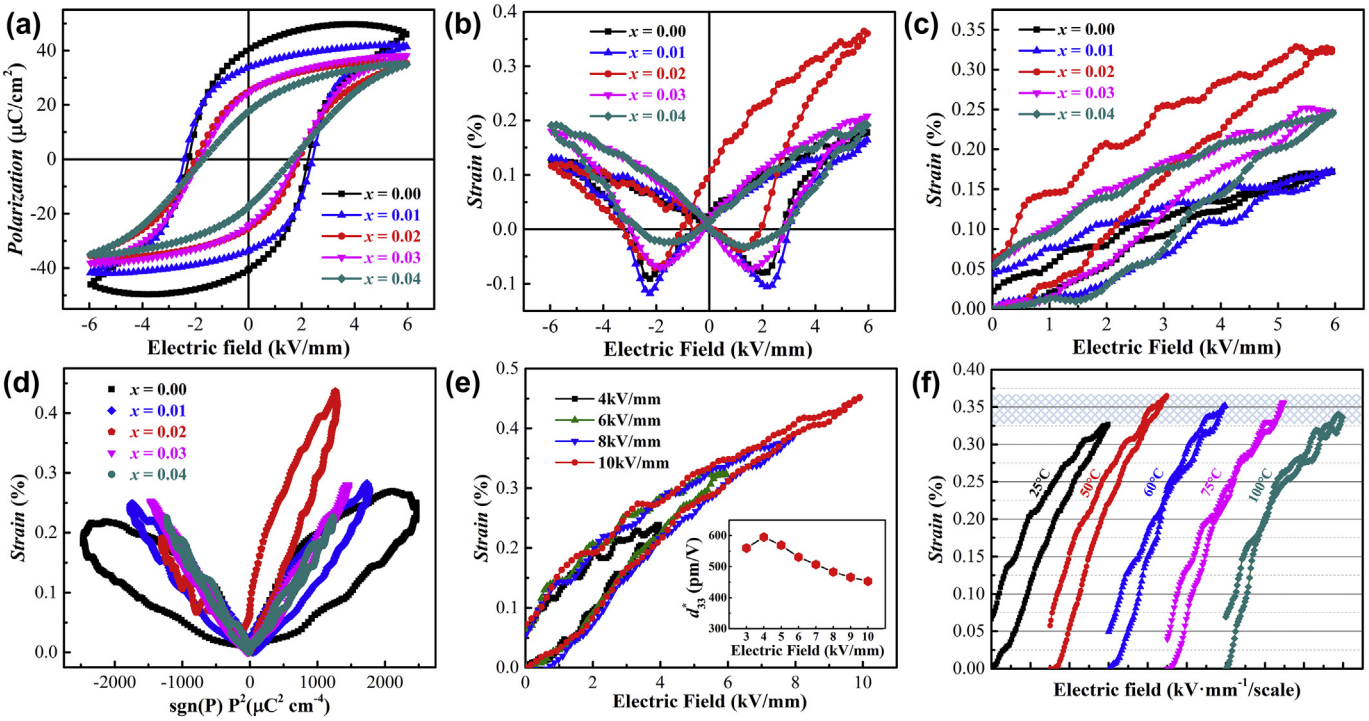

Fig. 2. Composition dependent bipolar *P-E* (a), *S-E* (b) and unipolar *S-E* curves, and strain as a function of P^2 (d) for BFBT-100*x*SLT ceramics. (e) Electric field dependent unipolar *S-E* curves (inset shows the normalized strain with varying electric fields) and (f) temperature dependent unipolar *S-E* curves at 6 kV/mm for $x = 0.02$.

The composition dependent bipolar hysteresis loops (*P-E*) and electrostrain curves (*S-E*) are shown in Fig. 2a and b. The remanent polarization (P_r) continuously decreased as SLT contents increasing, indicating that the ferroelectricity generally decreased with the addition of SLT. The bipolar strain curves show typical butterfly shape. Interestingly, a highly asymmetric strain loop was observed for $x = 0.02$, and it exhibited a large strain of 0.36% at the positive field of 6 kV/mm. Similar strain level was also observed in the unipolar strain curves. As shown in Fig. 2c, the unipolar strain was 0.33% for $x = 0.02$. Therefore, the enhanced unipolar strain is closely associated with the asymmetric bipolar strain characters. The asymmetric strain curves were commonly ascribed to internal bias electric field (E_{bias}) in ferroelectrics, formed by defect dipoles [15]. However, the E_{bias} of $x = 0.02$ was only 0.09 kV/mm, which is negligible as compared to its coercive field (~1.9 kV/mm). As the XRD results showed no any secondary phases in all samples, the asymmetric strain curves could be related to the defects at a microscopic level, which will be discussed latter.

The electrostrictive properties are a good indicator of relaxor characters. As shown in Fig. 2d, due to large strain hysteresis, broad *S-P* hysteresis were observed for $x \leq 0.02$. The electrostrictive coefficients generally increased as SLT contents increasing. It improved from 0.007 m^4/C^4 for $x = 0.00$ to 0.014 m^4/C^4 for $x = 0.02$. The $x = 0.03$ and $x = 0.04$ samples show typical electrostrictive behavior with large electrostrictive coefficients of 0.018 m^4/C^4, comparable to classical relaxor ferroelectric $Pb(Mg_{1/3}Nb_{2/3})O_3$ (0.015–0.023 m^4/C^4) ceramics [5]. The relaxor-like electromechanical behaviors are well commensurate with the diffuse dielectric characters.

Fig. 2e shows the electric field dependent unipolar strain curves for BFBT-0.02SLT sample. The maximum strain reached 0.45% with a relatively low strain hysteresis ($H = \Delta S_{hys}/S_{max}$) of 29% at 10 kV/mm at room temperature. The normalized strain ($d_{33}^* = S_{max}/E_{max}$) reached 600 pm/V at 4 kV/mm, as shown in inset of Fig. 2e. Fig. 3 shows the comparison of the electrostrain and depolarization temperature (T_d) and/or Curie temperature (T_C) with other representative piezoceramics. The present BFBT-0.02SLT samples possessed the highest T_C, a large electrostrain and a modest strain hysteresis. For example, KNN-based ceramics have low strain hysteresis, and yet with low strain level (<0.3%). The BNT-based ceramics showed high strain (≥0.3%), but they also exhibited low T_d (<100 °C) and large strain hysteresis (~60%). The temperature dependent unipolar *S-E* curves for BFBT-0.02SLT were presented in Fig. 2f. The variation of unipolar strain from 25 to 100 °C was only 10% of its room temperature value, which is thermally stable. The measured temperature range was limited by 100 °C due to leakage breakdown at higher temperature. Further modification needs to be conducted to improve the electrical insulation at high temperatures.

To provide a further insight into the structure on a short range, Raman spectroscopy was performed. According to the selection rule, R3c phases of $BiFeO_3$-based materials have 13 Raman-active modes:

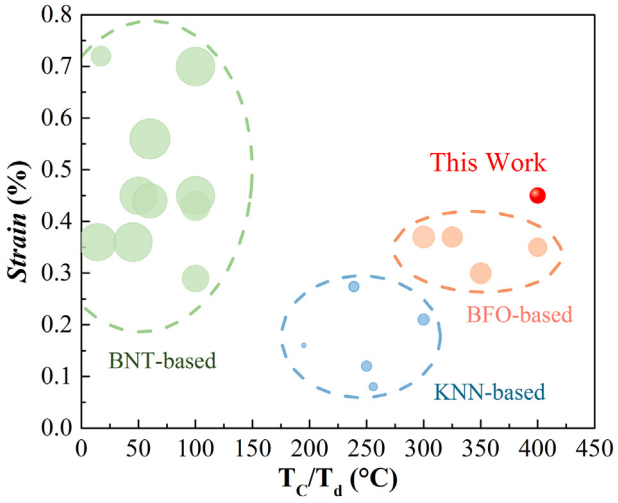

Fig. 3. Comparison of unipolar strain versus T_C/T_d with some representative BNT-[15–17,19,24–27], KNN-[3,18,28–30] and BFO-based [14,31–33] lead-free ceramics reported in the literature. The diameter of each circle is proportional to the strain hysteresis of each sample.

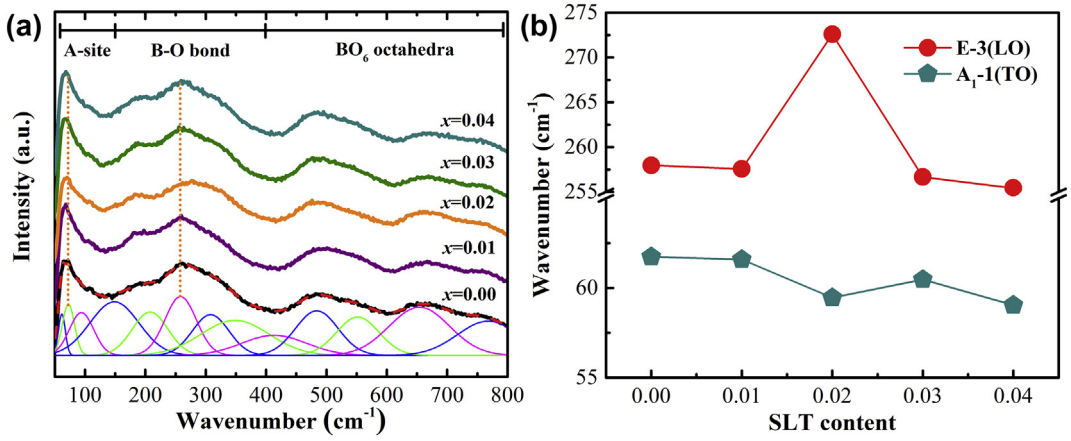

Fig. 4. Room temperature Raman spectra of BFBT-100*x*SLT with different compositions.

$\Gamma_R = 4A_1 + 9E$. As shown in Fig. 4, the measured Raman spectra of BFBT-100*x*SLT showed broaden peaks as compared to $BiFeO_3$. This is a clear indication of the coexistence of both short- and long-range polar orders [13,19]. Fig. 4b shows the peak positions of A_1-1(TO) and E-3(LO) modes, fitted by pseudo-Voigt (pV) functions. The addition of SLT affected both A-O and B-O vibrations. Obvious red shift (wavenumber decrease) of the A_1-1(TO) and E-3(LO) modes appeared with increasing SLT contents, which were consistent with the composition driven ferroelectric to relaxor phase transitions. An abrupt change in Raman shift appeared for BFBT-0.02SLT sample, with discontinuous wavenumber decrease of A_1-1(TO) mode and significant increase of E-3(LO) mode. As Raman shift is closely correlated with the crystal stress and polarization, the abrupt change is most likely related to the distorted local stress and polarization field. The modifier $Sr_{0.8}La_{0.1}\square_{0.1}TiO_{2.95}$ contains both A-site vacancies and oxygen vacancies for charge equilibration. Distorted stress field could be formed by these local defects. Therefore, both A-O and B-O vibrations were changed. At the critical composition of $x = 0.02$, apparent asymmetric bipolar strain curves were observed, indicating significant internal distortion field. As a result, the combined distortion field induced asymmetric bipolar strain curves and relaxor characters contributed to the enhanced unipolar strain effect of $x = 0.02$.

In summary, a composition driven ferroelectric to relaxor-like phase transition was observed in A-site deficient $Sr_{0.8}La_{0.1}\square_{0.1}TiO_{2.95}$ modified $0.67BiFeO_3$–$0.33BaTiO_3$ ceramics. The small addition of $Sr_{0.8}La_{0.1}\square_{0.1}TiO_{2.95}$ significantly improved electrostrain of the piezoceramics with slight decline of their Curie temperatures. A high unipolar strain of 0.45% with a high Curie temperature of 410 °C and relatively low strain hysteresis ($H = 29\%$) were obtained in BFBT-2SLT. Moreover, the unipolar strain was thermally stable in the measured temperature range, and the variation was only 10% from room temperature to 100 °C at 6 kV/mm. Electrostrain measurements showed an asymmetric bipolar strain curve for BFBT-2SLT. An abrupt change of Raman shift occurred for BFBT-2SLT, which may be due to the distorted crystal stress introduced by the A-site vacancies. By combining the electrostrain and Raman measurements, the enhanced strain effect can be attributed to the reduced energy barrier and distorted internal stress field, which were brought by the multivalence and vacancies on A-site. This study may provide an effective strategy to obtain high electrostrain in high temperature piezoceramics.

This work was jointly supported by the National Natural Science Foundation of China (Grant Nos. 11574334 and No. 11304334), the National Key Basic Research Program of China (973 Program, Grant No. 2015CB057502) and the Youth Innovation Promotion Association, Chinese Academy of Sciences (2016231).

References

[1] K. Uchino, Ferroelectric Devices, second ed. CRC Press, Boca Raton, 2009.
[2] W. Jo, R. Dittmer, M. Acosta, J. Zang, C. Groh, E. Sapper, K. Wang, J. Rödel, J. Electroceram. 29 (2012) 71–93.
[3] Y. Saito, Nature 432 (2004) 81–84.
[4] T.R. Shrout, S.J. Zhang, J. Electroceram. 19 (2007) 113–126.
[5] F. Li, L. Jin, Z. Xu, S.J. Zhang, Appl. Phys. Rev. 1 (2014), 011103.
[6] B. Narayan, J.S. Malhotra, R. Pandey, K. Yaddanapudi, P. Nukala, B. Dkhil, A. Senyshyn, R. Ranjan, Nat. Mater. 17 (2018) 427–431.
[7] J.R. Cheng, L.E. Cross, J. Appl. Phys. 94 (2003) 5188.
[8] P. Ravindran, R. Vidya, A. Kjekshus, H. Fjellvag, O. Eriksson, Phys. Rev. B 74 (2006), 224412.
[9] J.X. Zhang, Q. He, M. Trassin, W. Luo, D. Yi, M.D. Rossell, P. Yu, L. You, C.H. Wang, C.Y. Kuo, J.T. Heron, Z. Hu, R.J. Zeches, H.J. Lin, A. Tanaka, C.T. Chen, L.H. Tjeng, Y.H. Chu, R. Ramesh, Phys. Rev. Lett. 107 (2011), 147602.
[10] T. Rojac, A. Bencan, B. Malic, G. Tutuncu, J.L. Jones, J.E. Daniels, D. Damjanovic, J. Am. Ceram. Soc. 97 (2014) 1993–2011.
[11] S.O. Leontsev, R.E. Eitel, J. Am. Ceram. Soc. 92 (2009) 2957–2961.
[12] M.H. Lee, J.K. Da, J.S. Park, S.W. Kim, T.K. Song, M.H. Kim, W.J. Kim, D. Do, I.K. Jeong, Adv. Mater. 27 (2015) 6976–6982.
[13] J. Fu, R. Zuo, Acta Mater. 61 (2013) 3687–3694.
[14] D. Zheng, R. Zuo, J. Am. Ceram. Soc. 98 (2015) 3670–3672.
[15] X. Liu, X. Tan, Adv. Mater. 28 (2016) 574–578.
[16] T. Li, X. Lou, X. Ke, S. Cheng, S. Mi, X. Wang, J. Shi, X. Liu, G. Dong, H. Fan, Y. Wang, X. Tan, Acta Mater. 128 (2017) 337–344.
[17] K. Wang, A. Hussain, W. Jo, J. Rödel, J. Am. Ceram. Soc. 95 (2012) 2241–2247.
[18] Y. Wang, L. Hu, Q. Zhang, H. Yang, Dalton Trans. 44 (2015) 13688–13699.
[19] X. Liu, S. Xue, F. Li, J. Ma, J. Zhai, B. Shen, F. Wang, X. Zhao, H. Yan, J. Mater. Chem. C 6 (2018) 814–822.
[20] E. Iguchi, K.J. Lee, J. Mater. Sci. 28 (1993) 5809–5813.
[21] R. Shannon, Acta Crystallogr Sect A. 32 (1976) 751–767.
[22] K. Uchino, S. Nomura, Ferroelectrics 44 (1982) 55–61.
[23] T. Ozaki, S. Kitagawa, S. Nishihara, Y. Hosokoshi, M. Suzuki, Y. Noguchi, M. Miyayama, S. Mori, Ferroelectrics 385 (2009) 6155–6161.
[24] S.T. Zhang, A.B. Kounga, E. Aulbach, H. Ehrenberg, J. Rödel, Appl. Phys. Lett. 91 (2007) 112906.
[25] A. Hussain, C.W. Ahn, J.S. Lee, A. Ullah, I.W. Kim, Sens. Actuator A-Phys. 158 (2010) 84–89.
[26] A. Ullah, C.W. Ahn, A. Hussain, S.Y. Lee, I.W. Kim, J. Am. Ceram. Soc. 94 (2011) 3915–3921.
[27] W. Bai, Y. Bian, J. Hao, B. Shen, J. Zhai, J. Am. Ceram. Soc. 96 (2013) 246–252.
[28] F.Z. Yao, K. Wang, W. Jo, K.G. Webber, T.P. Comyn, J.X. Ding, B. Xu, L.Q. Cheng, M.P. Zheng, Y.D. Hou, J.F. Li, Adv. Funct. Mater. 26 (2016) 1217–1224.
[29] Z. Cen, Y. Huan, W. Feng, Y. Yu, P. Zhao, L. Chen, C. Zhu, L. Li, X. Wang, J. Mater. Chem. A 6 (2018) 19967–19973.
[30] Y. Yuan, J. Wu, H. Tao, X. Lv, X. Wang, X. Lou, J. Appl. Phys. 117 (2015), 084103.
[31] H. Matsuo, Y. Noguchi, M. Miyayama, M. Suzuki, A. Watanabe, S. Sasabe, T. Ozaki, S. Mori, S. Torii, T. Kamiyama, J. Appl. Phys. 108 (2010), 104103.
[32] G.H. Ryu, A. Hussain, M.H. Lee, R.A. Malik, T.K. Song, W.J. Kim, M.H. Kim, J. Eur. Ceram. Soc. 8 (2018) 4414–4421.
[33] S. Murakami, N. Ahmed, Da. Wang, A. Feteira, D.C. Sinclair, I.M. Reaney, J. Eur. Ceram. Soc. 38 (2018) 4220–4231.